Published in IET Microwaves, Antennas & Propagation
Received on 18th March 2009
Revised on 6th June 2009
doi: 10.1049/iet-map.2009.0102

ISSN 1751-8725

Phase noise degradation of varactor and BJT frequency multipliers in the presence of parametric instability

A. Ahmadi A. Banai F. Farzaneh

School of Electrical Engineering, Sharif University of Technology, P. O. Box 11365/9363, Tehran, Iran
E-mail: arash_ahmadi@ee.sharif.edu

Abstract: Varactor and bipolar junction transistor (BJT) frequency multipliers are a class of non-linear circuits that show parametric instability when the input drive is varied. If parametric oscillations are present in the circuit, output phase noise of the multiplier degrades remarkably in some specific driving levels. Phase noise analysis is performed by the conversion matrix method using generalised nodal analysis. The conversion method predicts the phase noise degradation precisely because it encompasses the effect of the noise sources that are modulated by the large signal drive. The added phase noise of a varactor and a BJT frequency doubler with subharmonic oscillation is calculated and the simulation results are compared with the measurements. Both simulation and measurements show phase noise degradation in the output spectrum in the presence of subharmonic oscillation.

1 Introduction

Frequency multipliers using varactor pn junction diodes and bipolar junction transistors are simple to design and are known as inexpensive solutions in the microwave range. In the presence of parametric instability, the output phase noise spectrum of the frequency multiplier can be degraded by more than the ideal $20 \log N$ dB, N being the multiplication factor [1].

When a pn diode junction is driven into forward conduction by a large signal, minority carrier holes are injected from the p layer into the n-layer. Because of the finite lifetime of the minority carriers in the n-layer, the diode continues to conduct if the cycle of the drive changes faster than the lifetime of the carrier. The delay of recombination of the carriers during the negative half cycle causes a dynamic negative resistance to appear across the diode terminals [2].

From a certain level of input drive power the negative resistance resonates with the passive components of the embedding network and parametric oscillation occurs [3].

The instability is observed in the frequency multipliers or dividers using varactor diode with finite life time, comparable to the period of the driving signal [2, 4]. Frequency multiplier circuits using Schottky barrier diodes, which are majority carrier devices, do not show parametric instabilities.

Because of the non-linearity in the capacitance of the Schottky barrier diodes, which is lower compared to varactor pn diodes, Schottky barrier diodes are used in a diode bridge and the action of frequency multiplication is accomplished by the switching of the diodes due to the large signal drive.

The phase noise spectrum of a non-linear circuit can be calculated by time domain or frequency domain methods. An earlier work drives the transfer function of amplitude and phase fluctuation of a varactor frequency multipliers, analytically [5]. The analytical equations describing the varactor frequency multiplier are based on simplifying assumptions and are solved finally by numerical methods.

The most famous time domain methods are based on Floquet's theory and the impulse sensitivity function [6].

The carrier modulation method and the conversion matrix method are the well known frequency domain methods for obtaining phase and amplitude noise in an autonomous or

forced non-linear circuit, based on harmonic balance [7]. In carrier modulation analysis, a mixed mode harmonic balance formulation is used with quasi-static assumption to obtain the near carrier phase noise spectrum of oscillators [7, 8]. The relation between the time and frequency domain techniques for phase noise analysis is compared in [6].

Conversion matrix method is a powerful frequency domain method for calculating phase noise spectrum of non-linear oscillators [7]. This method is also used to analyse the phase noise of non-linear circuits, in which frequency conversion takes place, like high frequency active and passive mixers [9, 10].

In [11] the conversion loss and noise figure of a Schottky diode frequency mixer are calculated, using conversion matrix method. The analysis includes internal noise sources of the diode, like shot noise and thermal noise sources. The equations for the analysis of the frequency mixer in [11] can be adopted to calculate the phase noise spectrum of a pn diode frequency multiplier. The phase noise spectrum of a varactor frequency multiplier is composed of frequency upconverted spectrum of the internal noise sources in the diode and the phase noise spectrum of the driving signal.

To perform the phase noise analysis, the phase noise spectrum of the input radio frequency (RF) signal and internal noise sources are considered as a sum of discrete, quasi-sinusoidal noise sideband components at specified offset frequencies. A pair of phase noise sideband components is applied to the linearised network and its effect on the output noise is investigated. Application of the conversion matrix method to a non-linear element like a diode, converts it to a linear multiport–multifrequency network. This network has ports at the harmonic frequency of the driving signal plus the offset frequency of the noise sidebands. The noise analysis of the frequency multiplier can be performed by reducing the multifrequency–multiport network to a four frequency–four port equivalent circuit, comprised of input and output noise sidebands [12]. The conversion matrix method is also called large signal-small signal method, because at first a large signal analysis like harmonic balance in the frequency domain or a time domain transient analysis is performed, neglecting the noise sources in the circuit and the noise of the driving signal.

Following the large signal analysis, the circuit is linearised around the driving waveforms and is excited by the small signal noise sources and noise sidebands of the driving signal.

If the multiplier circuit shows subharmonic oscillations, the harmonic balance method converges to a physically non-existent periodic solution, without the parametric oscillation [13]. The addition of an auxiliary generator at the oscillation frequency in the circuit with proper circuit conditions causes the results of harmonic balance method to converge to the correct and physically observable solution [4].

Time domain transient analysis takes all kinds of instabilities in the circuit into account and leads to the correct solution in the circuits comprised of non-linear elements and lumped components. The frequency spectrum of the parametric oscillation can be obtained by fast Fourier transform.

A combination of transient and harmonic balance method, called transient assisted harmonic balance method, is used by the advanced design system (ADS), which is a commercial software to calculate the frequency response of the circuits, in the presence of parametric oscillations. In this method at first a transient analysis is performed, then the results are used internally in the software to derive the properties of the auxiliary generator. After the frequency of parametric oscillation is known, a two tone harmonic balance analysis can be performed. In the case of subharmonic oscillation, a single tone harmonic balance analysis with a fundamental half of the frequency of the RF source is done. The prediction of the circuit behaviour of the multiplier under large signal drive is of prime importance because excessive phase noise degradation depends on the instabilities in the circuit.

Parametric oscillations are observed in some of the circuits like impact ionisation avalanche transit-time (IMPATT) oscillators, BJTs and Gallium Arsenide (GaAs) power amplifiers. In IMPATT oscillators, the oscillation acts as a pump to induce the negative resistance. The non-linear inductance of the avalanche zone can resonate with the loading circuit and, under certain conditions, results in parametric oscillation with half of the frequency of the initial oscillation. Under this condition the output noise spectrum of the oscillator degrades considerably [14].

The most observed parametric oscillation in the varactor frequency multiplier has a twice period of the driving signal. This is similar in IMPATT diodes and some GaAs power amplifiers [14, 15]. The mechanism of subharmonic generation in the BJTs is the base charge storage [15]. In metal semiconductor field effect transistor (MESFET) and junction field effect transistor (JFET) the carrier life time is extremely short compared with the period of the driving signal, because the charge transport in these devices is based on majority carriers. The parametric oscillation in MESFETs and JFETs is caused by the large signal drive of a non-linear element like the input capacitance of the device. The negative resistance is caused by the time varying reactive component and was originally predicted in [16]. The longer time constant of the charge storage in a BJT compared with the parametric mechanism in a FET or MESFET has a stronger effect in the generation of subharmonic oscillation in the non-linear circuits. Therefore circuits using a bipolar junction transistor as the frequency converting element are more subject to parametric instabilities when driven by a large signal pump.

In this paper the analysis of phase noise of a varactor and a BJT frequency multiplier with parametric instability is

presented. Because the equivalent non-linear circuit of a varactor diode is much simpler than a bipolar junction transistor, the multiplier circuit using a varactor is first studied. The results of the phase noise analysis in this circuit can be extended to circuits that are more complex, like a transistor frequency multiplier. In the first step a large signal analysis is performed in the non-linear multiplier circuit in the presence of the parametric oscillation by the transient assisted harmonic balance method. The multiplier circuit is then linearised by the conversion matrix method. Internal noise sources of the device like shot noise, flicker noise and thermal noise are taken into account. The behaviour of the output phase noise spectrum in the presence of the parametric oscillations is of the main concern. The results of the phase noise analysis are compared with measurements.

2 Varactor frequency doubler

To start the calculation of the phase noise spectrum of a frequency multiplier in the presence of parametric oscillation, a varactor diode in a frequency doubler circuit is analysed. The varactor used is BB535 from Infineon. The transit time of the minority carriers in the device is 120 ns. If the varactor frequency multiplier is driven hard by a large RF signal generator with a period comparable with the transit time of the device, parametric oscillations are observed.

The schematic of the frequency doubler is shown in Fig. 1.

The input RF signal frequency is 250 MHz. The frequency multiplier consists of a varacor diode, a three pole low pass filter of pass band 250 MHz as the input matching and an inductor/capacitor (LC) band pass filter of resonant frequency 500 MHz as the output matching network. The low pass filter consists of two series inductors and a shunt capacitor. This three element network matches the source resistance to the diode impedance and isolates the output circuit from the input circuit. The elements of the band pass filter are an inductor in series with a capacitor. A small reverse voltage is applied across the diode terminals through the biasing network.

In the schematic of Fig. 1 the parasitic components and resistive losses at the operating frequency are modelled and are used in the simulations.

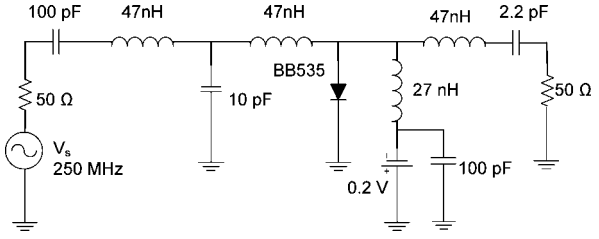

Figure 1 *Schematic of the varactor frequency doubler*

3 Noise sources in a pumped diode

The main noise sources in a varactor diode are thermal noise of the series resistance of the undepleted epi layer and contacts, shot noise and flicker noise of the barrier junction current. Shot noise and flicker noise are dependent on the diode barrier current. If the diode is driven by a high level harmonic signal, the statistical properties of these noise sources vary with the period of the driving signal. This effect is called modulation of the noise sources by the large signal waveform [17]. To formulate the concept of modulated noise in a pumped diode, the noise power spectral density is written as [7, 12]

$$S(v_b(t), i_j(t), f) = h^2(v_b(t), i_j(t))S_0(f) \quad (1)$$

where $S_0(f)$ is the time independent spectral power density and $v_b(t)$ and $i_j(t)$ are the barrier voltage and junction current, respectively.

The term $h(v_b(t), i_j(t))$ is the modulating function because of the large signal barrier voltage and junction current. Thus in a pumped diode, the statistical properties of the noise are function of time.

In time domain the corresponding noise process can be written as [18]

$$x(t) = h(v_b(t), i_j(t))x_0(t) \quad (2)$$

The noise source $x_0(t)$ represents a stationary noise process and $x(t)$ will be a cyclostationary noise source. The statistical averages and probabilities change with the period of large signal drive.

In the quasi-static approach the modulating function is expressed as a Fourier series [7, 18]. This time dependent function is the main cause of frequency conversion in the noise process.

The concept of frequency conversion can be understood by writing noise components $x(t)$ and $x_0(t)$ as the sum of narrow band sinusoidal components $\delta x(t,k)$ and $\delta x_0(t,k)$ in the incremental bandwidth $(f_0 + kf_p, f_0 + kf_p + \delta f)$, respectively [12]. f_p is the frequency of pumping signal, f_0 is the offset frequency and k is an integer; hence

$$x_0(t) = \sum_{k=-\infty}^{\infty} \delta x_0(t, k) = \sum_{k=-\infty}^{\infty} \mathrm{Re}\left[\sqrt{2}\delta X_0(k)e^{j2\pi f_k t}\right] \quad (3)$$

$$x(t) = \sum_{k=-\infty}^{\infty} \delta x(t, k) = \sum_{k=-\infty}^{\infty} \mathrm{Re}\left[\sqrt{2}\delta X(k)e^{j2\pi f_k t}\right] \quad (4)$$

doi: 10.1049/iet-map.2009.0102

where $\delta X_0(k)$ and $\delta X(k)$ are random complex rms values of narrowband sinusoidal noise components $\delta x_0(t, k)$ and $\delta x(t, k)$, respectively.

The vectors containing complex rms values $\delta X_0(k)$ and $\delta X(k)$ are linearly related by the conversion matrix of the periodic modulating function by substitution of (3) and (4) in (2) as written as

$$\delta \boldsymbol{X} = \boldsymbol{H}\delta \boldsymbol{X}_0 \tag{5}$$

where

$$\begin{aligned} \delta \boldsymbol{X}_0 &= \left[\ldots, \quad \delta X_0(1), \quad \delta X_0(0), \quad \delta X_0(-1), \quad \ldots\right]^{\mathrm{T}} \\ \delta \boldsymbol{X} &= \left[\ldots, \quad \delta X(1), \quad \delta X(0), \quad \delta X(-1), \quad \ldots\right]^{\mathrm{T}} \end{aligned} \tag{6}$$

$\boldsymbol{H}$ is the conversion matrix of the modulating function defined in (1). The computation is done by truncating the infinite summation in (3) and (4) from $-N$ to N so there are $2N+1$ sideband components in the analysis.

The correlation matrix of elementary noise is a diagonal matrix, composed of power spectral densities of the narrowband noise components times the noise bandwidth and is calculated as [12]

$$\begin{aligned} \boldsymbol{C}_{x_0} &= \overline{\delta \boldsymbol{X}_0 \cdot (\delta \boldsymbol{X}_0^*)^T} \\ &= \mathrm{diag}\left(\left[\ldots, \quad S_0(f_1), \quad S_0(f_0), \quad S_0(f_{-1}), \quad \ldots\right]\delta f\right) \end{aligned} \tag{7}$$

The correlation matrix of the modulated noise is computed by ensemble averaging of vector of narrow band modulated noise components and is given by

$$\boldsymbol{C}_x = \overline{\delta \boldsymbol{X} \cdot (\delta \boldsymbol{X}^*)^T} = \boldsymbol{H}\boldsymbol{C}_{x_0}\boldsymbol{H}^{\mathrm{T}} \tag{8}$$

In our analysis, we consider shot noise, flicker noise and thermal noise of the diode. Shot noise and flicker noise are represented by current noise sources across the barrier and thermal noise is represented by a voltage noise source in the undepleted part of the junction. The power spectral densities and modulating function of these noise sources are given in Table 1 [12].

All noise processes are independent and uncorrelated. Therefore the correlation matrix of the current noise sources across the barrier is the sum of individual correlation matrices of each current source across the barrier and is given by

$$\boldsymbol{C}_{\mathrm{i}} = \boldsymbol{C}_{\mathrm{shot}} + \boldsymbol{C}_{\mathrm{flicker}} \tag{9}$$

Table 1 Noise sources and the power spectral densities

Noise type	$x(t)$	$S_0(f)$	$h^2(v_b, i_j)$
shot	i_{sh}	$2q$	$i_b(v_b) + 2I_s$
flicker	i_{fn}	K_{fn}/f	$i_b(v_b)^2$
thermal	i_{th}	$4KT$	R_u

K is the Boltzman's constant, T is temperature in Kelvin, q is the electron charge and K_{fn} is the flicker noise factor. R_u is the resistance of the undepleted part of the junction.

4 Phase and amplitude noise analysis of the varactor frequency multiplier

Noise analysis of the diode frequency multiplier is performed by the conversion matrix method using the concept of conversion noise [7]. In this method at first a large signal simulation is performed. Then the circuit is linearised about the time varying operating point using the results of large signal analysis.

Large signal analysis of the diode multiplier is done in frequency domain by the method of harmonic balance without noise sources. The small signal analysis of the circuit with the linear time varying components and noise sources is done by the conversion matrix method.

The generalised nodal analysis is suitable for application of the conversion matrix method to a complicated network with arbitrary number of nodes. This method is general and there is no need to simplify the non-linear model of the device and noise sources in the circuit. The circuit of Fig. 2 is used for the nodal analysis of the frequency multiplier.

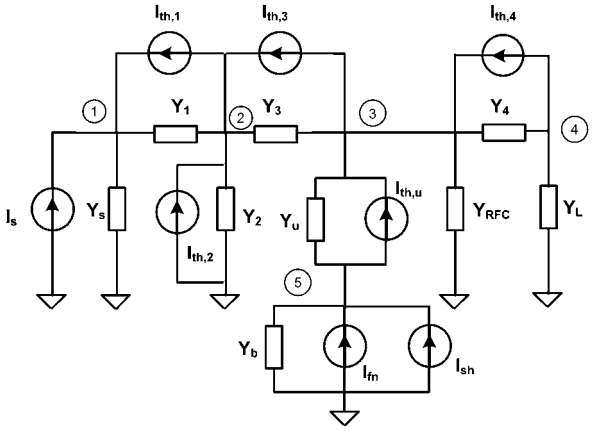

Figure 2 *Small signal circuit of the frequency multiplier used in nodal analysis*

$\boldsymbol{Y}_{\mathrm{u}}$ and $\boldsymbol{Y}_{\mathrm{b}}$ are the admittance conversion matrix of the undepleted epilayer and barrier of the diode, respectively. $\boldsymbol{Y}_{\mathrm{s}}$ is the conversion matrix of the source admittance, $\boldsymbol{Y}_1$, $\boldsymbol{Y}_2$, $\boldsymbol{Y}_3$, $\boldsymbol{Y}_4$ and $\boldsymbol{Y}_{\mathrm{RFC}}$ represent conversion matrices of the decoupling elements, components of the input and output filter and biasing choke. To generalise the calculations, these admittances can include parasitic elements and resistive losses. Each current noise source in Fig. 2 is a conversion vector of noise sources. The nodal voltage at each node in the circuit is a vector of noise sideband components and has the form of the noise sideband vector in (6).

Application of the nodal analysis to the circuit in Fig. 2 yields the following equation in matrix form (see(10)).

In general, (10) can be written as

$$\boldsymbol{Y}\boldsymbol{V}_{\mathrm{n}} = \boldsymbol{I}_{\mathrm{n}} \tag{11}$$

where $\boldsymbol{Y}$ is the conversion admittance matrix of the network. $\boldsymbol{V}_{\mathrm{n}}$ and $\boldsymbol{I}_{\mathrm{n}}$ are nodal voltage noise and nodal current noise of the network, respectively.

The nodal noise correlation matrix of the network is obtained by multiplying both sides of (11) by the transpose conjugate of each side and taking the statistical average of both sides. The resultant equation is given by

$$\boldsymbol{C}_{\mathrm{i,N}} = \boldsymbol{Y}\boldsymbol{C}_{\mathrm{v,N}}(\boldsymbol{Y}^*)^T \tag{12}$$

where $\boldsymbol{C}_{\mathrm{i,N}}$ and $\boldsymbol{C}_{\mathrm{v,N}}$ are the current noise correlation matrix and voltage noise correlation matrix of the network, respectively.

The thermal noise source due to the resistive part of each component is represented by a current source with a correlation conversion matrix as below [18]

$$\boldsymbol{C}_{\mathrm{th},k} = 4KT\delta f\ \mathrm{Re}\{\boldsymbol{Y}_k\} \tag{13}$$

where $\boldsymbol{Y}_k$ is the admittance conversion matrix of the corresponding element.

The modulated current noise sources due to flicker noise and shot noise across the barrier are characterised by their correlation matrices and are obtained by (8) and Table 1.

The thermal noise source in the undepleted part of the epilayer is modelled by a current source and has a correlation matrix similar to (13).

The following algorithm describes how the current noise correlation matrix of the network can be computed without writing the nodal equations of the circuit and avoiding the mathematical computations leading to (12).

If a current source is connected between node p and q, its source nodal matrix is defined as [19]

$$\boldsymbol{C}_{i_k;p,q} = \begin{bmatrix} \boldsymbol{C}_{i_k} & -\boldsymbol{C}_{i_k} \\ -\boldsymbol{C}_{i_k} & \boldsymbol{C}_{i_k} \end{bmatrix} \tag{14}$$

where $\boldsymbol{C}_{i_k}$ is the correlation matrix of the current noise source i_k. The submatrices of $\boldsymbol{C}_{i_k;p,q}$ are added to the submatrices of the current noise correlation matrix of the network by the following rule.

$$\begin{aligned} \boldsymbol{C}_{\mathrm{i,N};p,p} &= \boldsymbol{C}_{\mathrm{i,N};p,p} + \boldsymbol{C}_{i_k} \\ \boldsymbol{C}_{\mathrm{i,N};p,q} &= \boldsymbol{C}_{\mathrm{i,N};p,q} - \boldsymbol{C}_{i_k} \\ \boldsymbol{C}_{\mathrm{i,N};q,p} &= \boldsymbol{C}_{\mathrm{i,N};q,p} - \boldsymbol{C}_{i_k} \\ \boldsymbol{C}_{\mathrm{i,N};q,q} &= \boldsymbol{C}_{\mathrm{i,N};q,q} + \boldsymbol{C}_{i_k} \end{aligned} \tag{15}$$

where $\boldsymbol{C}_{\mathrm{i,N};m,n}$ is the submatrix of the mth row and nth column of the current noise correlation matrix.

If a current source is connected between ground and node p, its source nodal matrix will be

$$\boldsymbol{C}_{i_k;p} = \begin{bmatrix} \boldsymbol{C}_{i_k} & 0 \\ 0 & 0 \end{bmatrix} \tag{16}$$

In a similar way the contribution of this noise source is added to the current noise correlation matrix of the network. The voltage noise correlation matrix of the network is obtained by the following equation

$$\boldsymbol{C}_{\mathrm{v,N}} = \boldsymbol{Y}^{-1}\boldsymbol{C}_{\mathrm{i,N}}[(\boldsymbol{Y}^{-1})^*]^T \tag{17}$$

The voltage noise correlation matrix contains all information about the nodal voltage noises in the circuit. The output nodal conversion correlation matrix is a submatrix of the voltage noise correlation matrix. It is a matrix of dimension $(2N+1) \times (2N+1)$, where $2N+1$ is the total number of

$$\begin{bmatrix} \boldsymbol{Y}_{\mathrm{s}}+\boldsymbol{Y}_1 & -\boldsymbol{Y}_1 & 0 & 0 & 0 \\ -\boldsymbol{Y}_1 & \boldsymbol{Y}_1+\boldsymbol{Y}_2+\boldsymbol{Y}_3 & -\boldsymbol{Y}_2 & 0 & 0 \\ 0 & -\boldsymbol{Y}_2 & \boldsymbol{Y}_2+\boldsymbol{Y}_u+\boldsymbol{Y}_{\mathrm{RFC}}+\boldsymbol{Y}_4 & -\boldsymbol{Y}_4 & -\boldsymbol{Y}_{\mathrm{u}} \\ 0 & 0 & -\boldsymbol{Y}_4 & \boldsymbol{Y}_4+\boldsymbol{Y}_L & 0 \\ 0 & 0 & -\boldsymbol{Y}_u & 0 & \boldsymbol{Y}_{\mathrm{u}}+\boldsymbol{Y}_{\mathrm{b}} \end{bmatrix} \begin{bmatrix} \boldsymbol{V}_1 \\ \boldsymbol{V}_2 \\ \boldsymbol{V}_3 \\ \boldsymbol{V}_4 \\ \boldsymbol{V}_5 \end{bmatrix} = \begin{bmatrix} \boldsymbol{I}_{\mathrm{s}}+\boldsymbol{I}_{\mathrm{th},1} \\ \boldsymbol{I}_{\mathrm{th},2}-\boldsymbol{I}_{\mathrm{th},1}+\boldsymbol{I}_{\mathrm{th},3} \\ \boldsymbol{I}_{\mathrm{th},3}-\boldsymbol{I}_{\mathrm{th},2}+\boldsymbol{I}_{\mathrm{th,u}}+\boldsymbol{I}_{\mathrm{th},4} \\ -\boldsymbol{I}_{\mathrm{th},4} \\ \boldsymbol{I}_{\mathrm{fn}}+\boldsymbol{I}_{\mathrm{sn}}-\mathbf{I}_{\mathrm{th,u}} \end{bmatrix} \tag{10}$$

doi: 10.1049/iet-map.2009.0102

sidebands in the conversion method. The output node in our example is node number 4.

The elements of the correlation matrix of the output noise at sideband frequencies $f_l = f_0 - lf_p$ and $f_u = f_0 + lf_p$ are elements of the output voltage correlation matrix at the corresponding frequencies as shown in (18), where l is the multiplication factor.

$$\mathbf{C}_{v,4} = \begin{array}{c} \\ N \\ N-1 \\ \vdots \\ l \\ \vdots \\ 1 \\ 0 \\ -1 \\ \vdots \\ -l \\ \vdots \\ -N+1 \\ -N \end{array} \begin{array}{c} \begin{array}{cccccccccccc} N & N-1 & \cdots & l & \cdots & 1 & 0 & -1 & \cdots & -l & \cdots & -N+1 & -N \end{array} \\ \begin{bmatrix} & & & \vdots & & \vdots & & & & \vdots & & & \\ & & & & & & & & & & & & \\ \cdots & & & C_{ll} & & \cdots & & & & C_{lu} & \cdots & & \\ & & & & & & & & & & & & \\ & & & \vdots & & \vdots & & & & \vdots & & & \\ & & & & & & & & & & & & \\ \cdots & & & C_{ul} & & \cdots & & & & C_{uu} & \cdots & & \\ & & & & & & & & & & & & \\ & & & \vdots & & \vdots & & & & \vdots & & & \end{bmatrix} \end{array} \tag{18}$$

The noise voltage correlation matrix of the output node at sideband frequencies f_u and f_l is obtained by gathering the corresponding correlation elements shown in (18) into a new matrix called $\boldsymbol{C}_v^{ul}$ as follows

$$\boldsymbol{C}_v^{ul} = \begin{bmatrix} C_{uu} & C_{ul} \\ C_{lu} & C_{ll} \end{bmatrix} \tag{19}$$

The output phase and amplitude noise power spectral density is calculated by [12]

$$\boldsymbol{S}_{out}^{\varphi a} = \boldsymbol{M}^{-1}(V_0)\boldsymbol{C}_v^{ul}(\boldsymbol{M}^{-1}(V_0))^{-1} \tag{20}$$

where $\boldsymbol{M}$ is the modulating matrix relating narrow band sinusoidal rms phase and amplitude noise components to the resulting complex rms sideband noise components around a carrier of complex value X_o. The modulating matrix is defined as

$$\boldsymbol{M}(X_0) = \frac{1}{2}\begin{bmatrix} jX_0 & X_0 \\ -jX_0 & X_0^* \end{bmatrix} \tag{21}$$

The relation between narrow band sinusoidal rms phase and amplitude noise components to the complex rms sideband noise components is given by [12]

$$\begin{bmatrix} \delta X_u \\ \delta X_l \end{bmatrix} = \boldsymbol{M}(X_0)\begin{bmatrix} \delta\Phi \\ \delta A \end{bmatrix} \tag{22}$$

where δX_u and δX_l are sideband noise components at frequencies f_u and f_l about the carrier, respectively. $\delta\Phi$ and δA are phase and amplitude noise of the noisy carrier.

The effect of internal and external noise sources of the multiplier can be considered separately by splitting the current noise correlation matrix in (17) in two parts, containing the internal and external noise sources, separately as follows

$$\boldsymbol{C}_{v,N} = \boldsymbol{Y}^{-1}\boldsymbol{C}_{i,N;\,internal}[(\boldsymbol{Y}^{-1})^*]^T + \boldsymbol{Y}^{-1}\boldsymbol{C}_{i,N;\,generator}[(\boldsymbol{Y}^{-1})^*]^T \tag{23}$$

where $\boldsymbol{C}_{i,N;internal}$ is the current noise correlation matrix of the internal noise sources of the device and $\boldsymbol{C}_{i,N;generator}$ is the current noise correlation matrix due to phase noise of the signal generator.

5 Simulation and measurement results of the diode frequency doubler

The generalised conversion matrix method outlined in the previous section is applied to varactor frequency doubler circuit shown in Fig. 1. For the onset of parametric instabilities against input drive, a bifurcation analysis can be performed using transient assisted harmonic balance method of the ADS or by directly applying the method outlined in [4].

The simulated RF output power at the second harmonic and the output at half frequency power (subharmonic) against RF input power is shown in Fig. 3. A slight decrease of the output power with the onset of the subharmonic oscillation is observed due to bifurcation. The large signal analysis of the circuit is done by the ADS using harmonic balance method. In the large signal analysis the use of transient assisted harmonic balance ensures the convergence of the steady state solution to the stable physical behaviour of the circuit when subharmonic

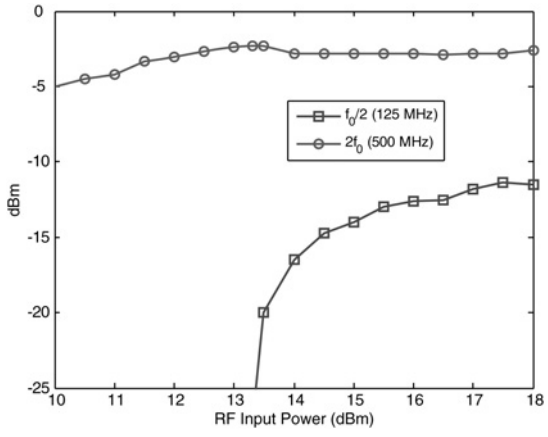

Figure 3 *Simulated second harmonic and half frequency output power versus RF input power in the varactor frequency multiplier*

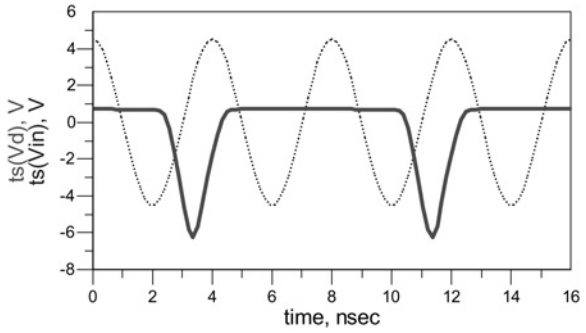

Figure 4 *RF input voltage (dotted line) and diode voltage (continous line) of the varactor frequency doubler in the presence of subharmonic oscillation*

oscillations are present. Fig. 3 shows parametric instabilities when the RF input power increases above 13.3 dBm.

A plot of RF input generator voltage and diode voltage with period doubling due to parametric instability is shown in Fig. 4.

For the phase noise analysis the flicker noise factor is taken to be 10^{-9}, which is a typical value for pn diode varactors of the same sort. The flicker noise power spectral density is assumed to vary as given in Table 1.

Fig. 5 shows phase noise degradation at 100 KHz offset from carrier against input power of the varactor frequency doubler. Both measurement and simulation of phase noise by conversion method show excessive phase noise degradation, just after subharmonic oscillation is observed in the circuit. In Fig. 5 a plot of the output phase noise degradation of the varactor frequency doubler is also shown when the internal noise sources of the device are taken to be non-cyclostationary.

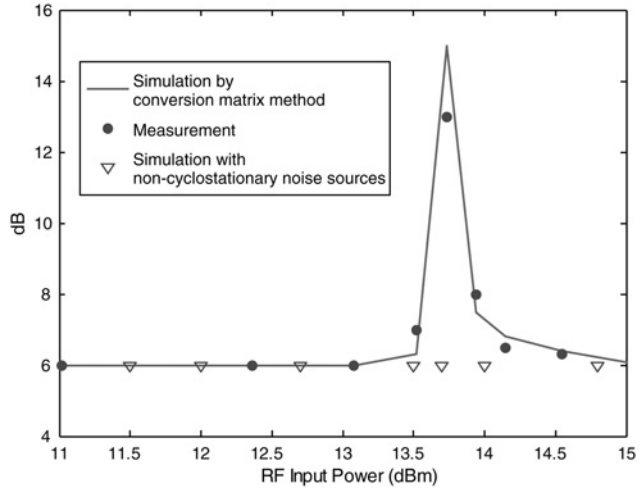

Figure 5 *Output phase noise degradation of the varactor frequency doubler*

The parasitic and resistive losses of the passive elements are modelled in the simulation. As shown, the results of measurements and simulations are in good agreement.

Phase noise spectrum of the RF signal generator and the simulated output phase noise spectrum of the frequency doubler are plotted in Fig. 6 for various RF drive levels.

Omitting the phase noise of the RF input signal source, thermal noise sources and diode shot noise in the simulation have minor effect on the excessive phase noise degradation, observed in the output.

Further examination on simulation results show that barrier current increases when parametric oscillation occurs. The increase of the barrier current causes flicker noise current to be highly modulated and the effective noise conversion increases significantly for a specified input RF drive.

If the phase noise of the RF source is relatively high, the observed phase noise in the output spectrum seems to be independent of the input power. In this case the output phase noise of the frequency doubler is 6 dB higher than the input, because the external phase noise of the multiplier circuit (noise due to the RF source) masks the internal added phase noise spectrum.

Fig. 7 shows the measured output phase noise spectrum of the frequency doubler for two RF input power levels. The spectrum analyser and the signal generator used for phase noise measurement were Agilent 8562EC and HP83752A, respectively. The output added phase noise is 14 dB at 100 KHz offset frequency from the 500 MHz carrier if the RF input power level is 13.7 dBm. For offset frequencies less than 30 KHz the phase noise of the signal generator entirely masks the internal noise sources of the device and

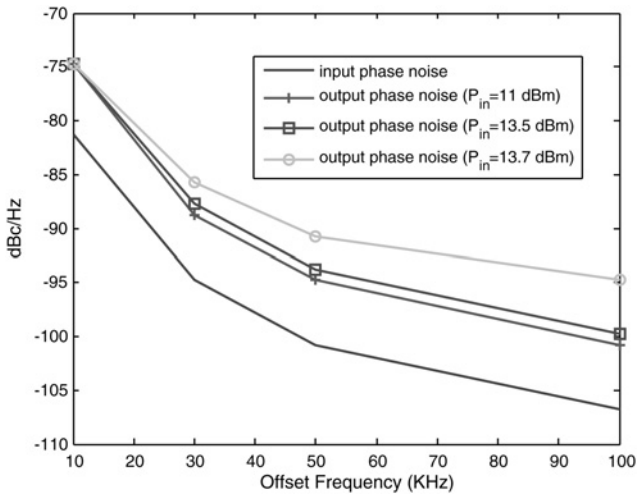

Figure 6 *RF signal generator phase noise spectrum and simulated phase noise spectrum of the frequency doubler for various RF input power levels*

doi: 10.1049/iet-map.2009.0102

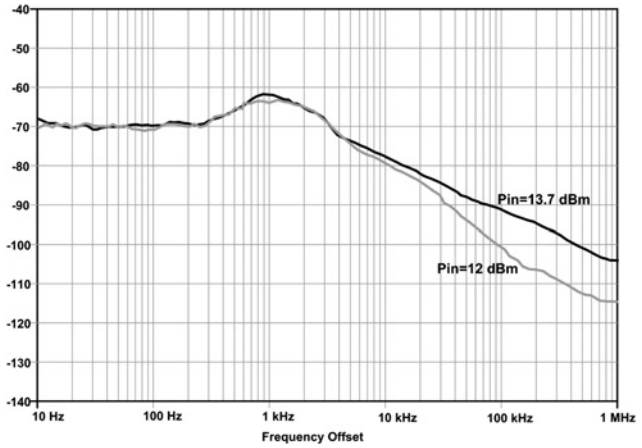

Figure 7 *Measured output phase noise spectrum of the frequency doubler for two RF input power levels*

phase noise degradation is not observed in the output phase noise spectrum.

The phase noise analysis of the varactor doubler shows that the frequency upconversion of the baseband flicker noise component to the corresponding sideband at the output frequency is the main cause of the excessive phase noise degradation at the output.

To further examine the effect of baseband noise upconversion, a small signal baseband sinusoidal signal is applied to the diode as shown in Fig. 8. In the output spectrum two sideband components around the carrier at an offset frequency equal to the frequency of the baseband signal appear. The magnitude of the sideband components relative to the output carrier is constant up to the point where parametric oscillation starts to grow up. At a specified RF input drive during start up of the parametric oscillation, the amplitude of the sideband components increases significantly and then decreases with further increasing RF input drive. Application of the generalised conversion matrix method to the circuit depicted on Fig. 8 shows similar results. Fig. 9 shows the result of the measured relative increase of the sideband components at the output due to the baseband source. For comparison

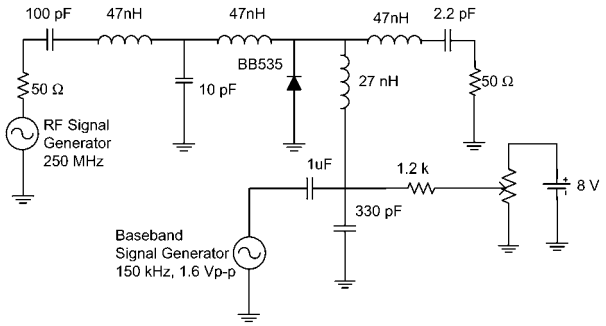

Figure 8 *Schematic of the varactor frequency doubler with the baseband modulating signal applied to the varactor diode*

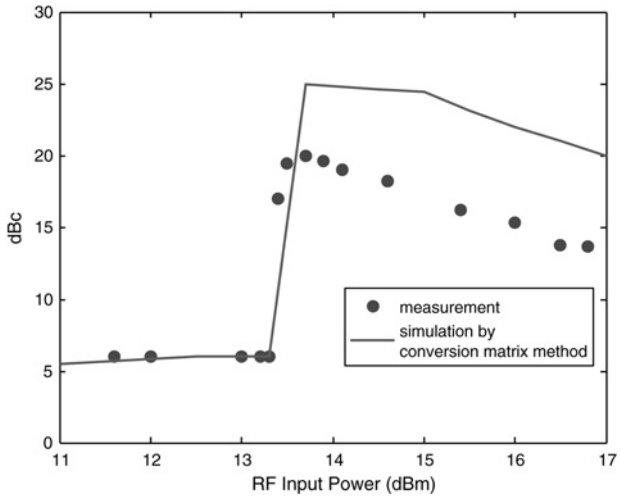

Figure 9 *Increase of the relative power of the output sideband components due to the upconverted baseband signal against input drive*

purposes the circuit in Fig. 8 is analysed with the conversion matrix method and the results are plotted in Fig. 9.

To examine the effect of the phase noise of the input RF signal generator on the output noise spectrum, the signal generator was externally frequency modulation (FM) modulated with low modulation index at a frequency of 150 kHz. With the aid of the FM-modulated RF source, the variation of the FM sideband in the output spectrum can be measured. Unlike the test performed on the circuit in Fig. 8 the amplitude of the FM sidebands in the output spectrum does not change, even if parametric instability is present or starts to grow up. This shows that the modulation of the internal baseband noise sources by the large signal current through the device is the main cause of the phase noise degradation in the output spectrum. Commercial simulators like ADS use the average barrier current in the expressions of the internal noise sources of the varactor, listed in Table 1. Simulating the frequency doubler in the ADS with static internal noise models, the output phase noise degradation shown in Fig. 6 cannot be observed, even if subharmonic oscillation is present in the circuit.

6 Simulation and measurement results of the BJT frequency multiplier

For the analysis of a BJT frequency multiplier, the 500 MHz frequency doubler circuit shown in Fig. 10 is used. This circuit consists of the matching circuit at the input and an LC resonator with a resonance frequency of 1 GHz in the output. The transistor used in the circuit is NE68830a, a well known low noise transistor from NEC. Application of the small signal stability analysis to

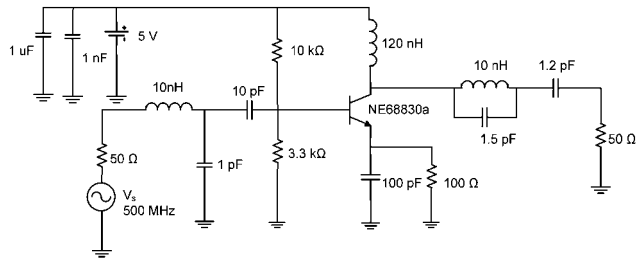

Figure 10 *Schematic of the BJT frequency multiplier*

the circuit shows unconditional stability. If driven hard by an external RF generator, the effective capacitance at the base emitter junction and base collector junction resonate with the net surrounding inductance of the bias and matching circuit. As a result, drive dependent subharmonic oscillation appears in the circuit. The frequency of the subharmonic oscillation equals half the frequency of the input drive. The simulated RF output power at the second harmonic and the output half frequency power (subharmonic) against RF input power is shown in Fig. 11.

Phase noise analysis of the BJT frequency doubler is done by the conversion matrix method mentioned in Section 4.

For the large signal analysis the Gummel–Poon model of the transistor was used [20]. The linear time variant circuit model used in the conversion matrix analysis is derived from the non-linear circuit model of the BJT frequency doubler and is depicted on Fig. 12. The noise sources in the pn junctions of the BJT are similar to the pn junction of a varactor. The package parasitic components and the parasitic components of the passive elements in the circuit are modelled in the phase noise

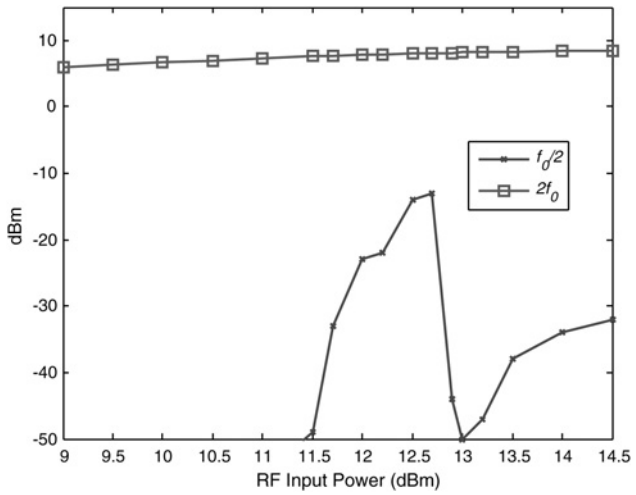

Figure 11 *Simulated second harmonic and half frequency output power against RF input power in the BJT frequency multiplier*

analysis. The selected transistor is a very low noise transistor. The flicker noise factor of this transistor is on the order of 10^{-12}.

The simulated output phase noise degradation of the BJT frequency doubler is plotted in Fig. 13 for two RF input power levels. The added phase noise for the RF input power level of 11.5 dBm is 10 dB compared to the 6 dB added phase noise, when the input power level is 4 dBm.

Fig. 14 shows the measured output phase noise spectrum of the BJT frequency doubler for three RF input power levels. The flicker noise factor of the selected BJT is lower compared to the varactor, so a very low phase noise RF signal generator must be used in the measurement of

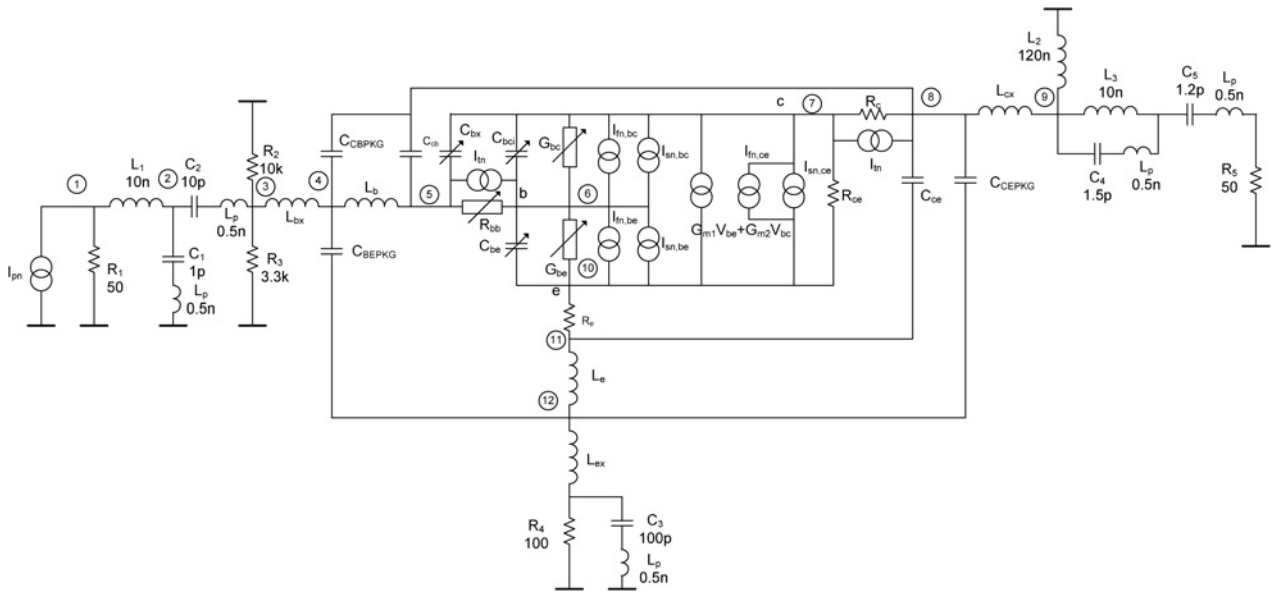

Figure 12 *Linear time variant circuit model of the BJT frequency doubler used in the conversion matrix analysis*

doi: 10.1049/iet-map.2009.0102

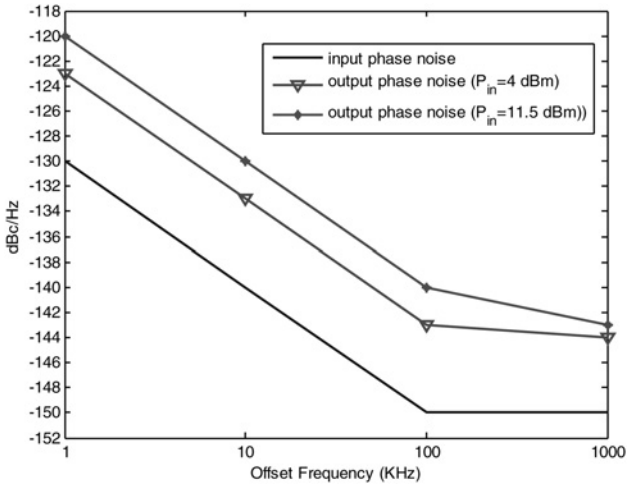

Figure 13 *RF signal generator phase noise spectrum and simulated phase noise spectrum of the BJT frequency doubler for two RF input power levels*

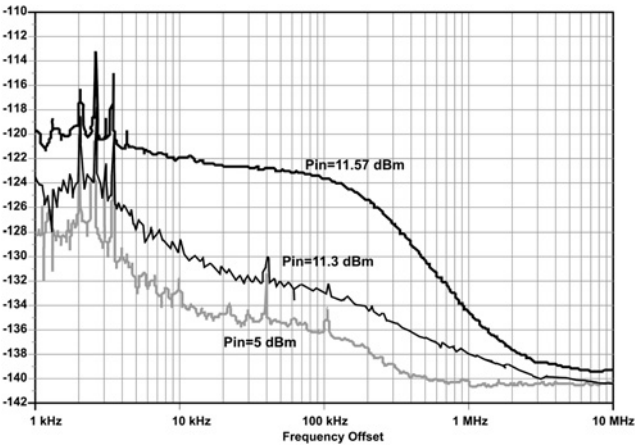

Figure 14 *Measured output phase noise spectrum of the BJT frequency doubler for various RF input power levels*

the output phase noise degradation. The RF signal generator used for this purpose is Agilent E8251A with −142 dBc/Hz phase noise at 100 KHz offset. The output phase noise spectrum was measured by the signal source analyser E5052A from Agilent. To measure the output phase noise spectrum in presence of the subharmonic oscillation an external band pass filter at the second harmonic of the input frequency was used between the BJT frequency doubler and signal source analyser. For harmonic termination and better isolation a 5 dB attenuator was used between the BJT frequency multiplier and the external band pass filter. The output added phase noise is 9 dB at 100 KHz offset frequency from the carrier, when the input power level is 11.3 dBm. At this input power level the subharmonic oscillation is starting to grow up. The RF input power can be fine tuned and its effect on the output phase noise degradation can be observed. At the input power level of 11.57 dBm the output added phase noise is

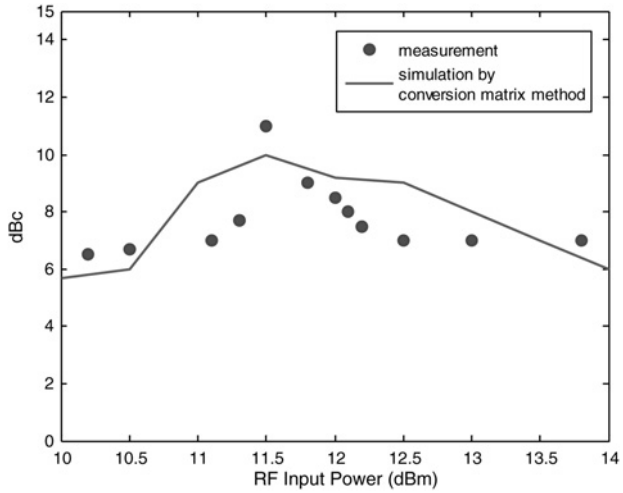

Figure 15 *Relative increase of the output sideband components due to the upconverted baseband signal*

18 dB at 100 KHz offset frequency. For slightly lower or higher RF input power levels the added phase noise at the output of the BJT frequency doubler is the expected 6 dB value.

The effect of the parametric instability on baseband phase noise upconversion in this circuit can be studied by connecting a baseband sinusoidal source to the base of the transistor. For this purpose a test circuit was built on FR-4 PCB material. The frequency of the baseband source is set at 150 kHz with a peak to peak voltage amplitude of 35 mV. For avoiding that the high frequency and bias conditions in the circuit be altered, the baseband source is connected via a series connection of a 1 μF capacitor and a 4 kΩ resistor to the base of the transistor.

Fig. 15 shows both the simulated and measured relative amplitude of the upconverted baseband signal in the output. The increase of the output sideband with the onset of parametric oscillation is similar to the case of the varactor frequency doubler.

The relative increase of the output sideband in the presence of parametric instability will not be observed if the BJT frequency doubler is driven by an FM-modulated RF source.

The degradation of phase noise spectrum in the presence of parametric oscillations is similar to the excess noise behaviour of the synchronised oscillators and dividers in the neighbourhood of synchronised band edges reported in [21, 22].

7 Conclusion

The conversion noise increases when subharmonic oscillations are present in the varactor and BJT frequency multipliers with a relatively high flicker noise factor. In the

case of a varactor frequency multiplier the added phase noise of the output spectrum at the second harmonic can become more than 14 dB higher at 100 KHz offset than the expected 6 dB value with respect to the input phase noise spectrum. In presence of subharmonic oscillation the output added phase noise of the BJT frequency doubler can increase up to 18 dB at 100 KHz offset frequency. The added phase noise is due to the internal sources especially the baseband flicker noise source in the pn junction, which is highly modulated by the large driving signal. The level of the output sidebands due to an upconverted baseband noise source, increases by the onset of parametric oscillations in both varactor and BJT frequency multipliers.

The added phase noise in the output spectrum due to internal noise sources are only observed if the phase noise of the RF source is relatively low.

The effect of the RF phase noise and the internal sources of the frequency multiplier on the output phase noise spectrum can be obtained with the conversion matrix method.

Conversion matrix method is a general method that does not need any use of reduced circuit models or some other simplifications, but requires more computer memory and time.

Commercially available softwares do not take into account the effect of modulation of the baseband noise sources, so excessive phase noise degradation in multiplier circuits is not observed by this kind of simulations.

8 Acknowledgment

The authors thank the Iran Telecommunication Research Center for its financial support of this work.

9 References

[1] AHMADI A., BANAI A.: 'Effect of parametric instability on phase noise degradation in a varactor frequency multiplier'. Proceedings of Asia-Pacific Microwave Conference, Bangkok, Thailand, 2007, pp. 1707–1710

[2] BASU S., MAAS S.A., ITOH T.: 'Stability analysis for large signal design of a microwave frequency doubler', *IEEE Trans. Microw. Theory Tech.*, 1995, **43**, (12), pp. 2890–2898

[3] SUAREZ A., JEON S., RUTLEDGE D.: 'Stability analysis and stabilization of power amplifiers', *IEEE Microw. Mag.*, 2006, **7**, pp. 51–65

[4] COLLANTES J.M., SUAREZ A.: 'Period doubling analysis and chaos detection using commercial harmonic balance simulators', *IEEE Trans. Microw. Theory Tech.*, 2000, **48**, (4), pp. 574–581

[5] BAVA E., PAOLO G., GODONE A., RIETTO G.: 'Analysis of varacor frequency multipliers: nonlinear behavior and hysteresis phenomena', *IEEE Trans. Microw. Theory Tech.*, 1979, **27**, (2), pp. 141–147

[6] SUAREZ A., SANCHO S., VER HOEYE S., PORTILLA J.: 'Analytical comparison between time- and frequency-domain techniques for phase-noise analysis', *IEEE Trans. Microw. Theory Tech.*, 2002, **50**, (10), pp. 2353–2361

[7] RIZZOLI V., MASTRI F., MASOTTI D.: 'General noise analysis of nonlinear microwave circuits by the piecewise harmonic balance technique', *IEEE Trans. Microw. Theory Tech.*, 1994, **42**, (5), pp. 807–819

[8] MEHRSHAHI E., FARZANEH F.: 'An analytical approach in calculation of noise spectrum in microwave oscillators based on harmonic balance', *IEEE Trans. Microw. Theory Tech.*, 2000, **48**, (5), pp. 821–831

[9] RIZZOLI V., MASOTTI D., MASTRI F.: 'Full nonlinear noise analysis of microwave mixers'. MTT-S Int. Microwave Symp. Dig., 1994, pp. 961–964

[10] MAAS S.A.: 'Theory and analysis of GaAs MESFET mixers', *IEEE Trans. Microw. Theory Tech.*, 1984, **32**, (10), pp. 1402–1406

[11] HELD D.N., KERR A.R.: 'Conversion loss and noise of microwave and millimeter wave mixers: Part1-Theory', *IEEE Trans. Microw. Theory Tech.*, 1978, **26**, (2), pp. 49–55

[12] FABER M.T., CHARAMIEC J., ADAMSKI M.E.: 'Microwave and millimeter-wave diode frequency multipliers' (Artech House, Boston, 1995)

[13] SUAREZ A., QUERE R.: 'Stability analysis of nonlinear microwave circuits' (Artech House, Boston, MA, 2003)

[14] RYDBERG A., LEWIN P.T.: 'An investigation of parametric noise in millimeter-wave IMPATT oscillator', *IEEE Trans. Microw. Theory Tech.*, 1987, **35**, (7), pp. 663–671

[15] IMBORNONE J.F., MURPHY M.T., DONAHUE R.S., HEANEY E.: 'New insight into subharmonic oscillation mode of GaAs power amplifiers under severe output mismatch condition', *IEEE J. Solid-state Circuits*, 1997, **32**, (9), pp. 1319–1325

[16] MANLEY J.M., ROWE H.E.: 'Some general properties of nonlinear elements-Part I. General energy relations'. Proc. IRE, July 1956

[17] KERR A.R.: 'Noise and loss in balanced and subharmonically pumped mixers: Part I-Theory', *IEEE Trans. Microw. Theory Tech.*, 1979, **27**, (12), pp. 938–943

doi: 10.1049/iet-map.2009.0102

[18] DRAGONE C.: 'Analysis of thermal and shot noise in pumped resistive diodes', *Bell Syst. Tech. J.*, 1968, **47**, (9), pp. 1883–1902

[19] MAAS S.A.: 'Noise in linear and nonlinear circuits' (Artech House, Boston, 2005)

[20] ANTOGNETTI P., MASSOBRIO G.: 'Semiconductor device modeling with SPICE' (McGraw-Hill, New York, 1993, 2nd edn.)

[21] COLLADO A., SUAREZ A.: 'Application of bifurcation control to practical circuit design', *IEEE Trans. Microw. Theory Tech.*, 2005, **53**, (9), pp. 2777–2788

[22] VER HOEYE S., SUAREZ A., SANCHO S.: 'Analysis of noise effects on the nonlinear dynamics of synchronised oscillators', *IEEE Trans. Microw. Compon. Lett.*, 2001, **11**, (9), pp. 376–378